Low-noise fiber-laser frequency combs (Invited)

Nathan R. Newbury* and William C. Swann

National Institute of Standards and Technology, 325 Broadway, Boulder, Colorado 80305, USA
**Corresponding author: nnewbury@boulder.nist.gov*

Received November 2, 2006; accepted December 19, 2006;
posted January 30, 2007 (Doc. ID 76696); published July 19, 2007

We discuss experimental and theoretical aspects of a low-noise fiber-laser frequency comb, including the experimental configuration and the major contributions to the frequency noise and linewidth of the individual comb modes. Intracavity noise sources acting on the mode-locked laser determine the free-running comb linewidth and include environmental changes, pump noise, and amplified spontaneous emission (ASE). Extracavity noise sources acting outside of the laser typically determine the signal-to-noise ratio on the comb lines and include environmental effects, shot noise, and noise generated during supercontinuum generation. Feedback strongly suppresses these intracavity noise contributions, yielding a system that operates with comb linewidths and timing jitter below the quantum limit set by the intracavity ASE. Finally, we discuss correlations in the residual noise across a phase-locked comb. © 2007 Optical Society of America

OCIS codes: 140.3510, 120.3930.

1. INTRODUCTION

Fiber-laser frequency combs have recently been the subject of a great deal of research and development [1–15]. They are based on the same principles as the solid-state Ti:sapphire frequency comb [16–19], namely, stabilizing all the individual modes of a passively mode-locked laser to a single microwave or optical reference (see Fig. 1). In the frequency domain, the stabilized output forms a comb of optical frequencies spanning a large spectral region, typically from 1 to 2 μm. One revolutionary application of frequency combs has been the precise measurement of optical frequencies; the frequency of a laser source is determined simply by measuring the frequency of its heterodyne beat against a given, well-defined, comb mode. This frequency metrology has clear applications to optical clocks [18], spectroscopy, and basic characterization of optical laser sources. Other potential applications include length metrology [20,21], coherent remote sensing [22], distribution of time and frequency over fiber networks [23,24], and the generation of stable microwaves [25]. For many of these applications, fiber-laser-based frequency combs are an attractive tool, and indeed there are several commercial products available [26,27]. Fiber-based frequency combs are relatively compact and robust compared to solid-state frequency combs. They cover a wavelength range that overlaps the optimum transmission window of optical fiber, the gain bandwidth of Er-based amplifiers, and the operating bandwidth of a wide array of fiber-optic components developed for telecommunications. To date, only Er-based fiber frequency combs have been demonstrated, but Yb-based fiber-laser frequency combs operating at 1 μm should be possible as well.

The general configuration of the frequency comb is shown in Fig. 2. It is based on a passively mode-locked fiber laser [28,29] that emits a pulse train in the time domain. This forms a frequency comb in the frequency domain, the "comb teeth" of which are just the modes of the mode-locked laser. These modes lie at optical frequencies given by the basic comb equation $\upsilon_n = nf_r + f_0$, where n is the mode number, f_r is the repetition frequency (the inverse of the pulse train period), and f_0 is the carrier-envelope offset frequency (see Fig. 1 and Refs. [16–19]). Left on its own, such a comb can drift in frequency space. Remarkably, however, stabilization of only 2 degrees of freedom of the comb automatically results in stabilization of all the comb modes [16–19]. The first attempt at stabilizing a fiber frequency comb was through locking a mode-locked fiber laser to a Ti:sapphire-laser frequency comb [30]. However since the first measurements of the comb offset frequency, f_0, in a fiber-laser system [31,32], present fiber-laser frequency combs have used self-referenced detection of f_0 to stabilize the comb. With the detection of f_0, the comb can either be locked directly to a single microwave reference [Fig. 1(a)] or to a single optical reference [Fig. 1(b)] [18,33,34] to form a stable comb of lines in frequency space. Fiber combs have developed rapidly from the first fully self-referenced, phase-locked system [1] to more compact f_0 detection [2], two-branch systems that permit access to visible wavelengths through frequency doubling [4], variable repetition rate combs [5], systems capable of operating for weeks and with excellent residual stability [6,13,15], combs with very low phase noise on the offset frequency [7,11,12], and finally to combs with subhertz residual linewidths [14].

The main performance metric of the frequency comb is how faithfully it reproduces the stability, phase noise, and linewidth of the reference to which it is locked across the teeth of the comb. Initial fiber frequency combs showed noisy performance; for example, the offset-frequency linewidth was ~100 kHz as opposed to the hertz-level linewidths achieved in solid-state frequency combs [35]. For applications in which the comb is locked to a microwave

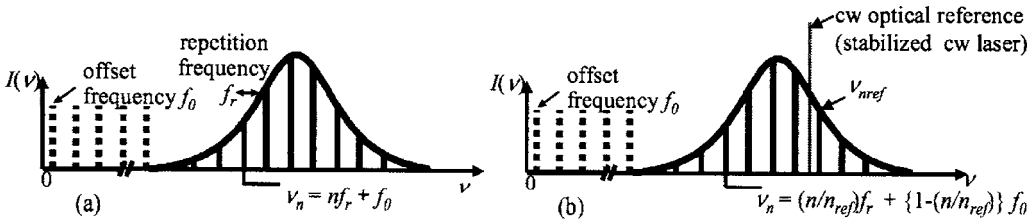

Fig. 1. Simplified schematic of the frequency comb output of a fiber-laser frequency comb. The comb teeth are simply the modes of the mode-locked laser. Supercontinuum generation after the laser extends this mode structure over a much wider spectral range (typically covering an octave of bandwidth) but the basic comb structure is preserved. The offset frequency, f_0, is detected by self-referenced detection. The comb can then be locked to (a) a microwave reference by locking f_r and f_0 to the reference or (b) an optical reference by locking one comb tooth at ν_{nref} to the optical reference and f_0 to a fixed fraction of the derived repetition rate.

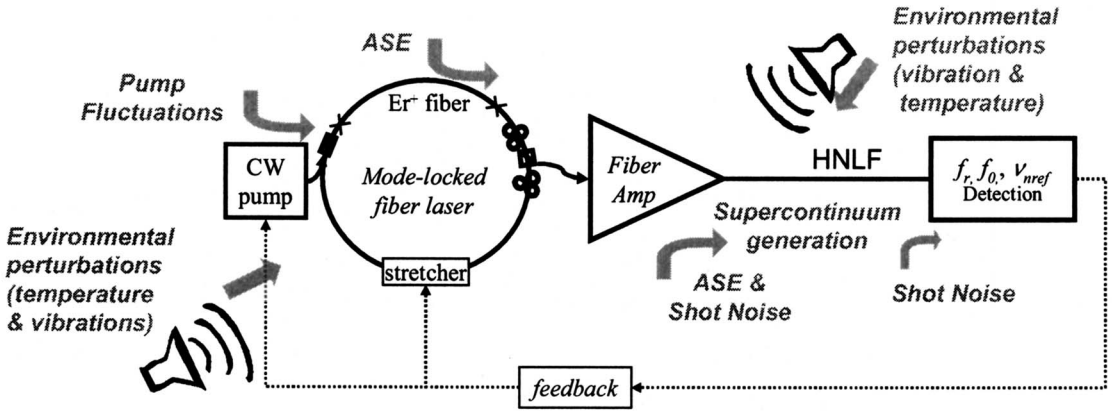

Fig. 2. Schematic of a fiber-laser frequency comb, which consists of a mode-locked fiber laser, Er-fiber amplifier, HNLF for supercontinuum generation, and detection of the offset frequency f_0, repetition frequency f_r, and frequency of an optical comb line ν_{nref} (through heterodyne detetection with a cw reference laser). The comb is stabilized through electronic feedback to the cavity length and pump power (shown as a dashed line). Noise sources are shown in gray. Intracavity noise acting directly on the laser includes environmental perturbations, ASE-induced quantum noise, and pump fluctuations. Extracavity noise acting after the laser includes environmental perturbations, shot noise, and excess phase noise generated during supercontinuum generation.

reference, this noise is unimportant since the average position of the comb line can still be counted far better than the stability of the microwave reference (typically $\sim 10^{-13}$ at 1 s). However, a number of applications require locking the comb to an optical reference. Examples include comparing state-of-the-art optical clocks and coherent lidar. In such cases, the linewidth and phase noise of the *optical* reference source should be faithfully transferred to each tooth in the comb; for a subhertz linewidth laser reference source, one would desire similar subhertz linewidths on the comb teeth (appropriately scaled by wavelength). Recently, a narrow linewidth, low phase-noise fiber-laser frequency comb has been demonstrated by first narrowing the offset-frequency linewidth [7,11,12] and then by phase locking a single mode to an optical reference [14]. The relative integrated phase noise on the individual modes, measured by comparing two such phase-locked combs, was ~1 rad on the ~200 THz optical carrier with a correspondingly instrument-limited linewidth. At these low noise levels, the fiber frequency comb operates below the quantum limit [36–38] on mode-locked fiber lasers imposed by amplified spontaneous emission (ASE) within the feedback bandwidth.

This paper discusses various noise sources that impact the frequency comb performance, describes our current low-noise fiber frequency comb system emphasizing those aspects important to low-noise operation, and finally addresses the issue of correlated noise across the phase-locked frequency comb. A number of noise sources that can perturb the comb are shown in Fig. 2. These noise sources can be divided into two groups: intracavity noise sources, which perturb the mode-locked laser itself, and extracavity noise sources, which act on the frequency comb after the laser. These various noise sources are reasonably well understood [8,9,11,12,36–42] and have very different effects on the comb.

The paper is organized as follows. Section 2 gives an overview of the physical configuration of a fiber frequency comb. Sections 3 and 4 discuss the various noise terms and quantify their impact on the free-running frequency comb in terms of both the tooth linewidth and the frequency noise power spectral density (PSD) on each tooth. Here we show that different noise sources of Fig. 2 will dominate, ranging from environmental noise to pump-induced noise to ASE-induced quantum noise to supercontinuum noise, depending on the optical frequency of the comb tooth and the Fourier frequency of the noise. Section 5 gives a more detailed description of our present frequency comb and compares its noise with the model of Section 3. Section 5 also provides some additional data on the in-loop performance of the fully phase-locked comb. Section 6 discusses the correlation of residual noise across

the comb. Appendix A includes a brief discussion of frequency noise PSDs and its connection with the comb linewidth.

2. OVERVIEW OF THE FIBER-LASER FREQUENCY COMB

A. Generating the Comb

The design of a fiber-laser frequency comb, given in Fig. 2, consists of five basic elements: (1) a passively mode-locked fiber laser, (2) an amplifier, (3) highly nonlinear fiber (HNLF) for supercontinuum generation, (4) photodetection of f_0 and either f_r or $f_{\text{beat}}=\nu_{opt}-\nu_{nref}$ (where ν_{opt} is the frequency of an optical reference and ν_{nref} is the frequency of an adjacent comb tooth), and (5) feedback electronics to the laser cavity length and pump power. A number of different laser designs have been successfully employed including a figure-eight laser [1], a soliton ring laser [9], a stretched-pulse fiber ring laser [3,4,14], a Fabry–Perot laser using a saturable absorber [2,7], and a simplified ring laser [13]. The direct output of the mode-locked laser produces a frequency comb over a 20–80 nm spectral width. The output pulses are amplified to ~1 nJ and injected into a piece of HNLF to generate a comb spanning from ~1 to ~2 μm [43,44].

B. Detection

Detection of f_r is easily accomplished by detecting a portion of the output pulse train. The full octave of spectral bandwidth of the comb from the HNLF permits detection of f_0 through the f-to-2f self-referencing technique [17,31,45]; the long-wavelength end of the supercontinuum is doubled and heterodyned against the short-wavelength end to produce a beat at f_0 as is easily verified by considering the basic equation $\upsilon_n=nf_r+f_0$ for the comb frequencies. This f-to-2f detection can be implemented with a standard Mach–Zehnder configuration [17], a collinear configuration [2,46], or a hybrid configuration, where the output of a collinear system is directed to a Mach–Zehnder interferometer. Theoretically, the offset frequency is defined as $f_0=\nu_c(1-\upsilon_{gr}/\upsilon_{ph})$, where ν_c is the carrier frequency, υ_{gr} is the average group velocity, and υ_{ph} is the average phase velocity of the cavity. For a fiber laser, this yields the experimentally inaccessible value of $f_0\sim 1-3$ THz [8,47]. However, f-to-2f detection actually generates an rf comb at $f_0\pm kf_r$ and experimentally we select one rf comb tooth at ~100 MHz, representing the "true" f_0 downshifted by the appropriate harmonic of the repetition rate. The distinction is typically unimportant provided one is consistent in using either the "theoretical" ~1–3 THz value for f_0 or the experimentally accessible ~100 MHz value.

C. Feedback Mechanisms and the Fixed Points

The final component in the comb is the feedback to the laser (shown as a dashed line in Fig. 2) to stabilize the comb. To define the mode frequencies with respect to a microwave reference, the modes are taken as $\nu_n=nf_r+f_0$ and both the repetition frequency, f_r, and offset frequency, f_0, are phase locked to the microwave reference [as in Fig. 1(a)] by feeding back to the cavity length and pump power, respectively. Alternatively, to lock to an optical reference, an individual comb line at ν_{nref} (with mode number n_{ref}) is locked to the optical reference by feeding back to the cavity length [as in Fig. 1(b)]. In that case, the comb modes are $\nu_n=r\nu_{nref}+(1-r)f_0$, where $r=n/n_{ref}$. To achieve a very low phase-noise comb with approximately hertz-level linewidths, only an optical reference will have the requisite phase coherence.

The action of the feedback on the comb modes is best described using the fixed-point formalism of Telle and coworkers [10,48]. In fact, this same fixed-point formalism is extremely useful in describing the various intracavity noise terms since it encompasses the correlations across the comb in a particularly compact manner and will be used later in Section 3. The basic idea is simple: changing a given parameter for the comb will cause the comb to expand or contract (or breathe) about a single fixed-point frequency, ν_{fix}. Different perturbations will have different fixed points and cause different magnitude of breathing of the comb. The fixed frequency ν_{fix} does not necessarily fall on a comb tooth or within the spectrum of the comb, but it will be finite except for the extremely rare case of a perturbation affecting only f_o and not f_r.

Mathematically, the fixed point is easily derived [10,28]. Consider a perturbation, δX, to one particular parameter of the mode-locked laser, X (in this case, the pump power or cavity length, but possibly the cavity loss, angle of a rotation plate, etc.). This perturbation will change the offset frequency by an amount $\delta f_0=(\delta X)\mathrm{d}_X f_0$, the repetition rate by an amount, $\delta f_r=(\delta X)\mathrm{d}_X f_r$, and the nth comb mode frequency by $\delta\nu_n\equiv n\,\delta f_r+\delta f_0$ (where d_X indicates a derivative with respect to X). This change in the comb mode frequency vanishes at $n_{fix}^X=-\mathrm{d}_X f_0/\mathrm{d}_X f_r$, so that the fixed point is simply $\nu_{fix}^X\equiv n_{fix}^X f_r+f_0$. The comb spacing will breathe about this point by an amount $\delta f_r=(\delta X)\mathrm{d}_X f_r$. One more comment is helpful. If the perturbation affects only the pulse round-trip time without affecting the carrier phase, the fixed point is at the carrier frequency. In other words, the mode near the carrier frequency is unperturbed, while the offset frequency (as the comb mode near zero) is strongly perturbed. On the other hand, a perturbation that shifts the carrier phase and arrival time commensurately has a fixed point at zero frequency. In other words, the mode at the carrier frequency is strongly perturbed, while the offset frequency is relatively unperturbed.

In addition to providing a satisfying intuitive picture of the comb response, the fixed point can be calculated from derived transfer functions (see Ref. [8], for example) or is easily measured experimentally [9] by applying a square wave to the given parameter, here the pump power or cavity length, and measuring the resulting change f_r and f_0. Figure 3 shows some example data used in determining the fixed points for pump power and cavity length changes of $\nu_{fix}^{\text{pump}}=206$ THz and $\nu_{fix}^{\text{length}}=1.0$ THz, respectively.

Since the fixed point for pump power modulation, ν_{fix}^{pump}, is near the carrier frequency, ν_c, any variations in the pump power are enormously leveraged in terms of their effect on the offset frequency; hence the pump power is used to control the offset frequency. Similarly, since the fixed point for cavity length variations is at low frequencies, any variations in the cavity length are enormously

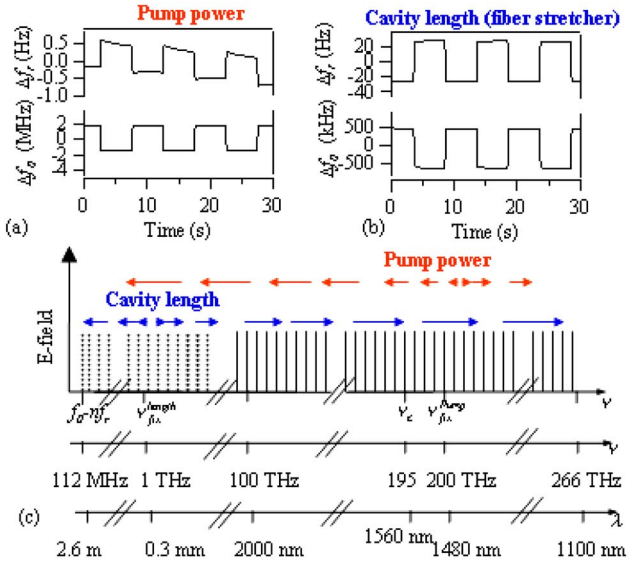

Fig. 3. (Color online) Example data illustrating the measurements of the fixed point for pump power and cavity length variations. (a) Counted change in f_r and f_0 in a 0.1 s counter gate time for a 0.1 Hz square wave in pump power. The sign of Δf_0 is ambiguous and must be determined by a separate reference laser. From these data, the fixed point is $\nu_{\mathrm{fix}}^{\mathrm{pump}}=(3.3\ \mathrm{MHz}/0.80\ \mathrm{Hz})\times 50\ \mathrm{MHz}=206\ \mathrm{THz}$ or 1460 nm. Also evident are a slow drift of the repetition rate and the thermal effects of changing the pump power. (b) Counted change in f_r and f_0 in a 0.1 s counter gate time for a 0.1 Hz square wave modulation of the cavity length. The fixed point is $\nu_{\mathrm{fix}}^{\mathrm{length}}=(1.1\ \mathrm{MHz}/53\ \mathrm{Hz})\times 50\ \mathrm{MHz}=1.04\ \mathrm{THz}$, as expected given the group and phase velocities of the optical fiber. Note that if an intracavity air path were used, the fixed point would be 0 Hz (see Subsection 4.A). (c) Schematic illustrating the effect of cavity length and pump-power variations given the measured fixed points. Solid lines indicate comb modes with optical power, dashed lines indicate projected comb modes with no optical power.

leveraged in terms of their effect on the optical frequencies; hence the cavity length is used to phase lock the relevant comb tooth at ν_{nref} to the optical reference. Tight phase locking requires high feedback bandwidth. For cavity length control, either a high-bandwidth piezoelectric transducer actuator [14] or an electro-optic phase modulator [49] can be used. For pump power control, the bandwidth can be extended using phase-lead compensation beyond the laser response bandwidth of ~10 kHz [11,12]. (In principle, other control parameters such as cavity loss, fiber birefringence, or cavity dispersion can provide feedback [8]; however, these approaches have not provided higher phase-locking bandwidth or dynamic range.)

A more detailed description of a fiber-laser frequency comb and its performance is given later in Section 5. For now though, we turn our attention to the noise sources that seek to disrupt the frequency comb.

3. NOISE AND LINEWIDTH ON A FREE-RUNNING COMB: OVERVIEW

The performance of the fiber frequency comb is determined by the noise on the comb lines. In this section, we summarize the dominant noise sources acting on the fiber comb including their physical origins and their effect on the frequency comb. The various noise sources were already introduced in Fig. 2 and can be divided into two groups: "intracavity" noise that affects the circulating laser pulse train and "extracavity" noise that affects the pulse train after the laser. Intracavity noise includes environmentally driven fluctuations in the cavity length and loss [8,36,37], pump-induced noise [11,12], and ASE-driven noise [36–38]. Extracavity noise sources include path-length fluctuations, shot noise from the limited power per comb tooth, and noise generated during supercontinuum generation [39–42]. These two noise groups differ significantly in their impact on the comb in two important ways.

First, the comb performance is much more sensitive to intracavity noise than extracavity noise. This sensitivity, as measured by the linewidth or frequency jitter, arises from the fact that the same perturbation that might cause white phase noise outside the cavity will cause white frequency noise inside the cavity. For example, a length change outside the laser cavity will causes a *phase* shift in the comb mode electric fields, while a length change inside the laser cavity will shift the repetition frequency and therefore cause a *frequency* shift in the comb modes. As a second example, ASE added outside the cavity by an amplifier will cause a white phase noise floor, while ASE added inside the cavity will cause white frequency noise, e.g., the "quantum-limited" frequency jitter on the repetition rate and individual comb modes. In summary, intracavity noise broadens the comb linewidth while extracavity noise decreases the comb "visibility" by increasing the noise floor.

Second, the intracavity noise is much better behaved than extracavity noise; intracavity noise can be described using the same fixed-point formalism discussed in Subsection 2.C, while extracavity noise in general cannot. Consequently the intracavity noise can usually be suppressed through feedback to the mode-locked laser while extracavity noise in general cannot. This simple behavior for intracavity noise follows from the fundamental assumption that the noise will perturb the pulse train only by modifying the pulse energy, carrier frequency, pulse arrival time, and carrier phase to lowest order [8,36]. (The pulse chirp can also be modified, but the effect of this modification is typically quite small [8].) It will not fundamentally break up the output pulse train or act on one comb mode to the exclusion of all others. This extremely powerful assumption is a result of assuming a consistent laser output [36] and has been effectively verified in tests of frequency comb stability conducted so far. In the frequency domain, the consequence is that the basic comb structure remains intact, so that intracavity noise simply introduces time dependence to the basic comb equation; the simple expression $\nu_n=nf_r+f_0$ becomes $\nu_n(T)=nf_r(T)+f_0(T)$, where T is a time slow compared with the cavity round-trip time [8]. Therefore, the noise on all the individual comb modes is completely determined by the noise on the repetition rate and offset frequency, which allows the use of the fixed-point model discussed earlier. [The effect of ideal supercontinuum broadening after the laser is only to "populate" more mode frequencies with actual light, so that the $\nu_n(T)$ cover more of the spectrum.] On the other hand, a given extracavity noise source can cause noise that varies in a complicated manner across the

comb that is incompatible with the expression $\nu_n(T) = nf_r(T) + f_0(T)$. As a simple example, consider the detection shot noise, which will be set by the power in an individual comb tooth. Since the amplitude of the supercontinuum output varies by orders of magnitude across the comb spectrum [see Fig. 2(b)], so will the detection shot noise floor. Some extracavity noise, such as external pathlength fluctuations, that are common mode to the entire comb can, however, be reduced by feedback. The effect of the two categories of noise terms is emphasized in Fig. 4.

To develop a quantitative picture of the noise, we will use the frequency noise power spectral density. We can begin by observing that noise causes an individual mode frequency to fluctuate with time, $\delta\nu_n(T)$. Just as with rf oscillators [50], these fluctuations can be characterized by the PSD, $S_{\nu n}(f) = \langle \delta\tilde{\nu}_n^2 \rangle$ in $\mathrm{Hz}^2/\mathrm{Hz}$, where the tilde represents a Fourier transform with respect to T and f is the Fourier conjugate variable. This frequency noise PSD describes a jitter of the comb tooth n at a modulation frequency f with a variance of $S_{\nu n}(f)$. Equivalently, the phase noise PSD, $S_{\varphi n}(f) = f^{-2} S_{\nu n}(f)$ describes the fluctuations on the phase of the comb mode. See Appendix A for more details.

The total frequency noise PSD from multiple, uncorrelated noise sources is calculated by simply adding up the noise PSDs from the various sources, giving

$$S_{\nu n} = (\underbrace{S_{\nu n}^{\mathrm{length}} + S_{\nu n}^{\mathrm{loss}} + S_{\nu n}^{\mathrm{pump}} + S_{\nu n}^{ASE}}_{\text{intracavity noise}}) + (\underbrace{S_{\nu n}^{supercontinuum} + S_{\nu n}^{\text{shot noise}} + S_{\nu n}^{\mathrm{length},ext}}_{\text{extracavity noise}}), \quad (1.1)$$

where the dependence of each PSD on Fourier frequency, f, is suppressed.

The intracavity noise is described by the first four terms: length fluctuations $S_{\nu n}^{\mathrm{length}}$ [8,38], loss fluctuations $S_{\nu n}^{\mathrm{loss}}$ [8], pump noise $S_{\nu n}^{\mathrm{pump}}$ [11,12], and ASE quantum noise $S_{\nu n}^{ASE}$ [36–38], (and for simplicity, we assume the environmentally induced loss and length terms are uncorrelated). As discussed above, each of these intracavity noise terms can be described using the fixed-point formalism (See Subsection 2.C and Refs. [10,48]) as

$$S_{\nu n}^{X} = (\nu_n - \nu_{\mathrm{fix}}^{X})^2 S_r^X(f), \quad (1.2)$$

where $S_r^X(f) = f_r^{-2}(\widetilde{\mathrm{d}_X f_r})^2 S_X(f)$ is the PSD of the fractional repetition-rate fluctuations driven by the fluctuations in the parameter X, and $\nu_{\mathrm{fix}}^X \equiv n_{\mathrm{fix}}^X f_r + f_0$ is the "fixed point" for that given parameter. This formalism has the advantage of avoiding the otherwise awkward inclusion of a cross-correlation term $(\mathrm{d}_X f_0)(\mathrm{d}_X f_r)$. Equation (1.2) describes the breathing motion of the comb about the fixed points, pictured in Fig. 4. It also includes the fact that this motion can roll off with high modulation frequencies depending on the spectral shape of $S_r^X(f) = f_r^{-2}(\widetilde{\mathrm{d}_X f_r})^2 S_X(f)$, which in turn depends on the Fourier-frequency dependence of the laser response $(\widetilde{\mathrm{d}_X f_r})$ (i.e., the transfer function between perturbations in X and the repetition rate) and the Fourier-frequency dependence of the noise source $S_X(f)$.

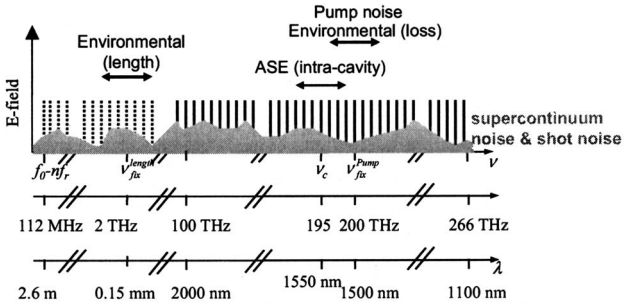

Fig. 4. Schematic showing the effect of various noise terms on the comb. Solid lines indicate comb modes with optical power, dashed lines indicate projected comb modes with no optical power. Intracavity noise sources (environmental length and loss fluctuations, pump noise and ASE-induced noise) cause frequency jitter, which is well described by a breathing motion of the comb about a fixed frequency. The jitter increases quadratically as one moves away from the fixed point. Depending on the noise, the jitter will decrease at higher modulation frequencies (which is not captured in this figure). The extracavity noise causes a strongly varying phase noise floor and is more difficult to quantify. Note the fixed point for the length fluctuations differs from Fig. 3 since here we assume all the fiber in the cavity is equally stretched whereas for the fiber stretcher only the properties of the fiber being stretched were important.(Also see Fig. 4 of Ref. [38]).

The extracavity noise is described by the remaining three terms: excess noise during supercontinuum generation, $S_{\nu n}^{\mathrm{supercontinuum}}$ [42], shot noise, $S_{\nu n}^{\text{shot noise}}$, and length fluctuations, $S_{\nu n}^{\mathrm{length},ext}$. The supercontinuum noise and shot noise can be grouped together since they both result in white phase noise, which raises the overall noise floor as depicted in Fig. 4.

The frequency noise predicted from Eq. (1.1) is plotted in Fig. 5 at three different points across the comb, corresponding to $\nu_n = 0$, $c/(1535\ \mathrm{nm})$, and $c/(1126\ \mathrm{nm})$. The contribution from each individual PSD term in Eq. (1.1) is summarized in Table 1. For each individual PSD contribution to the noise, the scaling with Fourier frequency, f, and with optical frequency, ν_n, is given by the formulas in Section 4. The overall magnitude of each component is varied to fit with the experiment. In Section 4, these fitted values are compared with the values expected based on theory.

Several trends are evident in the overall PSD plots given in Fig. 5. In general, the frequency noise is dominated by environmental effects at low frequency, by pump noise for low-middle range of frequencies, quantum-limited noise for higher frequencies, and ultimately by the white phase noise contribution from supercontinuum noise or shot noise for even higher frequencies. The exact transition frequencies between the various dominant mechanisms will depend on the position across the comb. For example, at the wings of the comb (1 or 2 μm), environmental noise dominates below 500 Hz, pump noise dominates from 0.5–50 kHz, quantum-limited noise dominates from 50–500 kHz, and supercontinuum and shot noise from 500 kHz and up. Near the center of the comb (1.5 μm), environmental noise dominates up to 50–100 kHz, and supercontinuum and shot noise dominates for higher frequencies.

Lasers are often specified by their linewidth. In some cases, the quoted laser linewidth is the Lorentzian linewidth inferred from the white frequency noise at large

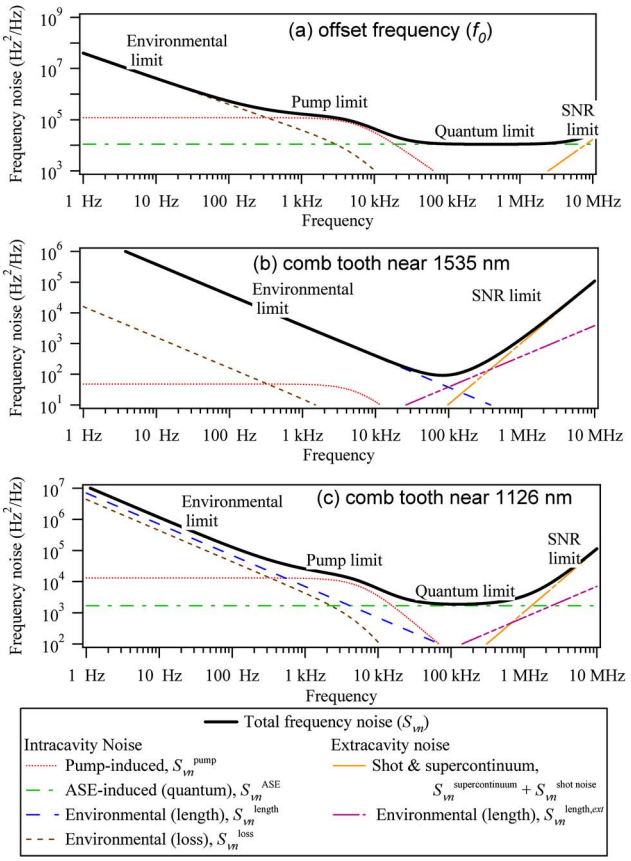

Fig. 5. (Color online) Calculated frequency noise PSD for a free-running comb for the mode at (a) f_0, (b) 1535 nm, (c) 1126 nm. The total contribution (thick, black curve) comprises the three intracavity contributions: pump noise, ASE-induced quantum noise, and environmental fluctuations (on both cavity length and loss); and two extracavity contributions: environmental fluctuations and the combined effect of shot noise and excess noise generated during supercontinuum formation. This last term is directly connected with the SNR ratio of the measured signal and thus is labeled as "SNR limit" in the graphs. The SNR ranges from 43, 35, and 35 dB in a 300 kHz bandwidth for plots (a)–(c) (chosen to agree with data presented later). Other values used in the plots are listed in Table 1.

Fourier frequency offsets, rather than a FWHM; this method can seriously underrepresent the FWHM width by not incorporating low-frequency jitter. Here, we consider the FWHM linewidth. Since the frequency noise typically diverges at low Fourier frequency (i.e., $1/f$ noise), we must furthermore specify an observation time for the linewidth, taken as 1 ms in Fig. 6. In general, a numerical calculation is required to generate the linewidth from the frequency noise PSD, $S_{\nu n}$, but various analytical approximations do exist for simple PSD shapes (see Appendix A). Figure 6 gives the linewidths across the comb based on the frequency noise PSDs in Fig. 5. As also shown in Refs. [11,12], the pump-induced noise is expected to dominate the linewidths away from the comb center.

Section 4 describes each term in Eq. (1.1) in more detail. In particular, while the fixed-point picture is useful in picturing the comb motion for intracavity noise, it does not tell us the values for fixed-point ν_{fix}^X and magnitude and spectral shape of the repetition-rate fluctuations S_r^X. The results of Section 4 are also summarized in Table 1.

4. INDIVIDUAL NOISE TERMS

A. Intracavity Noise: Pump Induced

The Er gain medium in the laser is pumped by a Fabry–Perot, fiber-Bragg-grating stabilized diode laser at either 980 or 1480 nm. These pump lasers exhibit both technical $1/f$ and white amplitude noise that will cause noise on the comb mode frequencies. In Ref. [8], the effect of pump power on the mode frequencies was analyzed using a moment-based perturbation theory and the master equation for a soliton fiber laser. The exact same effects will be present in a stretched-pulse laser, since they are fundamental to the propagation of a pulse around the laser cavity, and could be similarly derived starting from the master equation. Instead, we can follow the general development in Section 2 of Ref. [8], to write down the sensitivity of the repetition frequency to slow changes in the pump power, P, for either a solitonic or stretched-pulse laser as [8,9]

$$\left(\frac{df_r}{dP}\right)_0 = -f_r^2\left[\beta_2\frac{d\omega_c}{dP} + \omega_{rms}\beta_3\frac{d\omega_{rms}}{dP} + \Omega_g^{-1}\frac{dg}{dP} + \frac{\delta}{\omega_c}\frac{dA^2}{dP}\right], \tag{1.3}$$

where the first term results from the change in the round-trip time due to the net cavity dispersion, β_2, coupled with pump-induced shifts in the carrier frequency, $\omega_c = 2\pi\nu_c$. These frequency shifts can be further delineated as a Raman self-frequency shift and a shift due to a frequency-dependent loss. The second term results from the change in the round-trip time due to the net third-order cavity dispersion, β_3, coupled with pump-induced shifts in the rms spectral width, ω_{rms}. The third term results from the resonant contribution from the Er gain assuming a Lorentzian gain shape with peak value g and bandwidth Ω_g. The derivative dg/dP will depend strongly on the effective nonlinear loss in the laser. The final term is the nonlinear self-steepening contribution from the lumped fiber nonlinearity, δ, and the peak of the electric field envelope A. The exact value of the derivative dA^2/dP will depend on the coupling between the pulse energy and width and therefore will depend on the laser dynamics (i.e., whether it is solitonic, dispersion-managed soliton, stretched pulse, etc.) but will be proportional to A^2/P. For a fiber-laser system this last term is typically of negligible amplitude [8]. In addition to the timing shifts, the carrier phase will have some power dependence, $d\varphi/dP$ through self-phase modulation and through a resonant contribution to the index of refraction from the Er gain medium (which only vanishes for a truly Lorentzian gain profile). The overall sensitivity of the offset frequency is $df_0/dP = -(2\pi)^{-1}(\beta_0 df_r/dP + f_r d\varphi/dP)$. The ratio of this value to Eq. (1.3) gives the mode number and finally the frequency of the fixed point [9],

$$\nu_{\mathrm{fix}}^{\mathrm{pump}} = \nu_c + f_r\left(\frac{d\varphi}{2\pi dP}\right)\Bigg/\left(\frac{df_r}{f_r dP}\right)_0 \approx \nu_c, \tag{1.4}$$

which is typically equal to the carrier frequency as indicated since the second term is typically $\ll \nu_c$ [8], although it is possible that the various terms in Eq. (1.3) almost cancel such that $df_r/dP \to 0$ and the fixed point moves sig-

Table 1. Fixed Point, Frequency Dependence, and Magnitude of the Various Contributions to the Frequency Noise on the Comb Lines

Noise Term	Fixed Point (ν_{fix})	Frequency Dependence	Magnitude at $f=1$ Hz $S_r(1)$ in Units of 1/Hz	Suppress by
Environmental (length)[a,b]	0–3 THz (1 THz)	f^{-1}	10^{-22}	Environmental isolation
Environmental (loss or pump power)	ν_c (200 THz)	$\{f(1+(f/f_{3\,dB})^2)\}^{-1}$ $f_{3\,dB}=5-10$ kHz[c]	10^{-21}	Environmental Isolation, reduce $f_{3\,dB}$
Pump noise	$\sim\nu_c$ (200 THz)	$\{1+(f/f_{3\,dB})^2\}^{-1}$ $f_{3\,dB}=5-10$ kHz	3×10^{-24}	Reduce pump RIN and cavity $f_{3\,dB}$
Intracavity ASE (quantum limit)	$\sim\nu_c$ (190 THz)	f^0	3×10^{-25}	Reduce effective cavity loss
Supercontinuum and shot noise[d]	NA[c]	f^2	6×10^{-23} to 6×10^{-24}	Higher peak powers
Environmental (external path length)[e]	0–2 THz	f	10^{-32}	Minimize extra path lengths

[a]These values are used in calculating the frequency noise PSD at any point across the comb. The values in parentheses for the fixed point are the values used in Figs. 5, 6, and 8. The magnitude of the repetition rate noise is expressed in terms of the fractional noise on the repetition rate.

[b]The actual dependence will vary from a strict $1/f$ rolloff.

[c]$f_{3\,dB}=6$ kHz for the plotted values in Figs. 5 and 6.

[d]For the purposes of calculating the frequency noise from the given $S_r(1)$, assume an effective fixed point of 0 THz, so that the total contribution is $f^2(\nu_n/f_r)^2S_r(1)$. This choice is purely a notational convenience to include this term in the table.

[e]As in *b*, the actual frequency dependence of the length fluctuations will vary from a strict $1/f$ rolloff and therefore the effect on the frequency noise will vary from a simple linear dependence on f. The magnitude will vary strongly with experimental conditions.

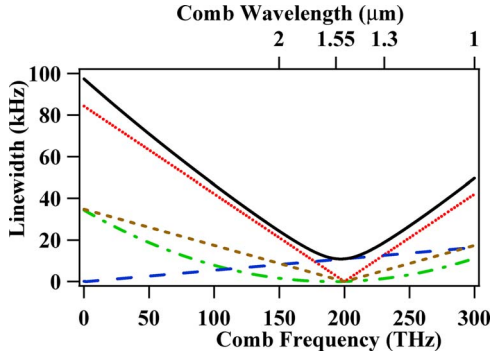

Fig. 6. (Color online) Linewidth across the comb. The total linewidth (solid black curve) has a dominant contribution from the pump noise (red, dotted curve) with additional contributions from the quantum limit (green, dashed-dotted curve), and environmental $1/f$ noise from cavity length fluctuations (blue, long dashed curve) and cavity loss fluctuations or $1/f$ pump fluctuations (brown, short dashed curve). The values and color coding used in these graphs are identical to those in Fig. 5. The contribution of the $1/f$ noise is calculated over an (arbitrary) time window of 1 ms. The total linewidth is approximated as the sum in quadrature of the individual components. The extracavity noise terms do not contribute significantly to the linewidth. The linewidth of the measured offset frequency beat is simply the value at ~0 THz.

nificantly from the carrier frequency [9]. (In contrast, a model for a dispersion-managed solitonic laser with no fiber or resonant gain dispersion includes only the weak self-steepening effect and self-phase modulation, which are of comparable magnitude so that the fixed point is far from the carrier frequency [51].)

Since the number of terms in Eq. (1.3) makes an exact calculation difficult, it is safest to simply measure the fixed point and the value of $(df_r/dP)_0$ using the technique illustrated in Fig. 3. The laser's response to pump fluctuations will roll off with increasing Fourier frequency beyond the characteristic low-pass frequency cutoff of $f_{3\,dB}$ so that the PSD describing the fractional frequency fluctuation in terms of the pump laser relative intensity noise (RIN), $S_{RIN\text{pump}}$, is [11,12]

$$S_r^{\text{pump}}(f) = B\frac{1}{1+(f/f_{3\,dB})^2}S_{RIN\text{pump}} \quad [1/\text{Hz}], \qquad (1.5)$$

where the measured value of $B=(Pdf_r/f_rdP)_0^2\sim4\times10^{-11}$ and $f_{3\,dB}\sim6$ kHz (see Ref. [12] or Fig. 3). Equations (1.4) and (1.5) are used in Eq. (1.2) to generate the appropriate contribution to the full PSD, Eq. (1.1). A pump RIN of $S_{RIN\text{pump}}$ of −131 dBc/Hz yields the fitted value $S_r^{\text{pump}}(f)$ used in Table 1 and Fig. 5.

B. Intracavity Noise: Environmental Perturbations

There are a number of possible environmental effects on the mode-locked laser including cavity length changes through thermal effects on the fiber or baseplate, vibrationally induced length changes, thermally induced birefringence changes, vibrationally induced changes in the cavity loss, etc. We consider two effects here: a cavity length change and a cavity loss change. In addition to the dependence of the comb on pump power, Ref. [8] gives transfer functions, equivalent to the derivatives d_Xf_0 and d_Xf_r, versus cavity length or loss. These give a fixed point for length change of

$$\nu_{\text{fix}}^{\text{length}} = \nu_c\left(1 - \frac{v_{\text{group}}^L}{v_{\text{phase}}^L}\right) = 0 \text{ to } 3 \text{ THz}, \quad (1.6)$$

where ν_c is the carrier frequency, and $v_{\text{group (phase)}}^L$ is the group (phase) velocity associated with the added cavity length. Again this result is independent of whether the laser is solitonic or stretched pulse. If the added cavity length has exactly the same group and phase velocities as the cavity, then $\nu_{fix}^{\text{length}} = f_0 \approx 2$ THz. (The "theoretical" value for f_0 discussed in Subsection 2.B.) If the added cavity length is in an air path, then $\nu_{fix}^{\text{length}} = 0$. For a general fiber stretcher, $v_{\text{group}}^L < v_{\text{phase}}^L$, and the fixed point is $\sim 0.01\nu_c$ ($\ll$ the carrier frequency $\nu_c = 200$ THz). This expression [Eq. (1.6)] assumes that the change in length is not associated with any cavity loss or change in cavity birefringence, both of which will move the fixed point (see below for a discussion of the cavity loss). The associated fractional noise in the repetition frequency is

$$S_r^{\text{length}}(f) = \left(\frac{f_r}{v_{\text{group}}^L}\right)^2 S_{\text{length}}(f) \quad [1/\text{Hz}], \quad (1.7)$$

which falls off roughly as $1/f$ in Fourier frequency. For temperature changes, we consider S_{length} to describe the "effective" length changes in the fiber ΔL given by $\Delta L/L = 10^{-5}\,\text{K}^{-1}$. Equations (1.6) and (1.7) are used in Eq. (1.2) to calculate $S_{\nu n}^{\text{length}}$ in Eq. (1.1). The value of $S_r^{\text{length}}(f) = 10^{-22}/f$ in Table 1 corresponds to $S_{\text{length}}(f) = 1.6 \times 10^{-3}/f$ (nm^2/Hz), which could be attributed to the quite low temperature fluctuations of $S_T = 1/f$ ($\mu\text{K}^2/\text{Hz}$) in the kilohertz region. (At lower Fourier frequencies, this noise will increase dramatically as shown in Fig. 8.)

For a cavity loss change, the effect is similar to that from pump noise, discussed above, and is difficult to distinguish from $1/f$ pump noise. However, we include it simply to show that the environmental fluctuations can cause noise with dramatically different character (i.e., completely different fixed points and spectral PSD shapes), depending on whether the cavity length or loss is affected. As with the pump-induced noise, the fixed point is typically near the carrier frequency:

$$\nu_{fix}^{\text{loss}} \approx \nu_c. \quad (1.8)$$

Assuming gain dispersion dominates, the fractional frequency fluctuations f_r are

$$S_r^{\text{loss}}(f) = B\frac{1}{1 + (f + f_{3\text{ dB}})^2} S_{\text{loss}}(f)[1/\text{Hz}], \quad (1.9)$$

where the PSD describing the S_{loss} fluctuations is expected to fall off as $1/f$ and B is defined as in Eq. (1.5). The value of $S_r^{\text{loss}}(f)$ in Table 1 corresponds to $S_{\text{loss}} = 2.5 \times 10^{-11}/f$, although at least a portion of this noise could equally well be attributed to $1/f$ noise on the pump power.

C. Intracavity Noise: Amplified-Spontaneous-Emission-Induced Noise (Quantum-Limited Noise)

The effect of ASE was first analyzed by Hauss and Mecozzi [36] for soliton lasers using soliton perturbation theory. Later, Paschotta [37] and Paschotta *et al.* [38] pointed out that the ASE-induced noise is not specific to solitonic lasers but can be derived for any general shaped laser pulse essentially using a moment method [52]. In that vein, the formalism of Ref. [8] can also be used to yield the same results as in Ref. [37]. ASE-induced noise is sometimes referred to as the "quantum limit" for the noise of the mode-locked laser since the ASE ultimately arises from quantum vacuum fluctuations. (This limit is separate from the quantum limit resulting from shot noise on the output laser pulse.)

The ASE will add to the pulse as it circulates around the cavity, leading to fluctuations in the pulse energy, carrier phase, frequency, and timing. These fluctuations are uncorrelated so that there is not a single fixed point to describe all effects. (Returning to the simple derivation of the fixed point, the ASE has effectively infinite degrees of freedom and cannot be described by a single parameter, X.) However, we can consider the ASE-induced noise in terms of two overall noise sources: a timing jitter and a phase jitter [37,38]. The timing jitter dominates the comb linewidth away from its fixed point, which must be at the carrier frequency,

$$\nu_{fix}^{ASE,\text{timing}} = \nu_c, \quad (1.10)$$

and drives fractional fluctuation in the repetition frequency about this point of [36–38,53]

$$S_r^{ASE,\text{timing}}(f) = 2f_r^2\left(\frac{(1 + n_{sp})h\nu G}{P_{circ}}\right) \times \left[t_{rms}^2 + \left(\frac{\beta_2}{4D_g\omega_{rms}}\right)\right] \quad [1/\text{Hz}], \quad (1.11)$$

where G is the cavity power gain (equal to the cavity loss), n_{sp} is the effective spontaneous emission factor averaged over the length of the Er-doped fiber [54] to which 1 is added to effectively account for the quantum noise from cavity loss [55], P_{circ} is the circulating laser power, β_2 is the net cavity dispersion, and D_g is the gain dispersion. The first term in brackets results directly from the ASE-induced timing jitter, and the second term results indirectly from the ASE-induced frequency jitter coupled with the cavity dispersion. To account for either a sech^2 pulse shape from a solitonic laser or a Gaussian-like shape from a stretched-pulse laser, the expression is written in terms of the rms pulse width, t_{rms}, and the rms spectral width, ω_{rms}. (For a highly stretched-pulse laser an appropriately averaged value of the rms widths is needed.) Strictly speaking the second term rolls off near f_r along with the carrier frequency fluctuations [8]. Additional nonlinear effects are negligible. Unlike the pump-power induced noise, Eq. (1.5), this expression is independent of f, which is, experimentally, the only strongly observable difference between the two.

For completeness, we note the additional phase noise jitter leads to the Schawlow–Townes limit, which is the same for all modes [56], and is [37,38]

$$S_{\nu n}^{ASE,ST} = 2\frac{f_r^2}{(2\pi)^2}\left(\frac{(1 + n_{sp})h\nu G}{P_{circ}}\right) \quad [\text{Hz}^2/\text{Hz}], \quad (1.12)$$

which is typically negligible compared to other noise terms.

The value of $S_r^{ASE,\text{timing}}(f)=3\times10^{-25}$ quoted in Table 1 and used in Fig. 5 was chosen to agree with experiment. We can compare with the value expected from Eq. (1.11). Based on the pump power of ~110 mW, the laser output power of ~8 mW, and an assumed quantum efficiency of 70% for the 1480 nm pump, the overall gain (or loss) of the cavity is $G=(110/8)(0.7)(1480/1560)\sim10$, a result of intracavity loss, nonoptimal gain length, and spectral broadening outside of the gain window. The effective value of $n_{sp}=2$ corresponds to a 6 dB noise figure for the Er gain section, which is not unreasonable for a 1480 nm pump and operation well into gain saturation. For $P_{circ}=10$ mW and a rough estimate of the average rms pulse width for the intracavity stretched pulse of $t_{rms}=400$ fs, $S_r^{ASE,\text{timing}}(f)=3\times10^{-25}$.

D. Extracavity Noise: Environmental Terms

Environmentally induced fiber or air path length changes outside the cavity will also cause noise. If the offending path length change is within the feedback path of the system, it can be removed, but invariably there are "out-of-loop" paths that are uncompensated, contributing a fractional frequency noise of

$$S_{\nu n}^{\text{length},ext}(f)\approx\left(\frac{2\pi f\nu_n}{v_{ph}}\right)^2 S_{\text{length}}(f)\quad[\text{Hz}^2/\text{Hz}]. \quad (1.13)$$

For simplicity, we have ignored dispersion, which will shift the fixed point to the terahertz regime. Assuming a 3 m patch cord with an effective coefficient of thermal expansion of 10^{-5}/K and external temperature noise of $\sim0.01/f\,(\text{mK})^2/\text{Hz}$ for kilohertz Fourier frequencies, then $S_{\nu n}^{\text{length},ext}(f)=(10^{-32})\nu_n^2 f\,\text{Hz}^2/\text{Hz}$, as quoted in Table 1 and used to generate Fig. 5 from Eq. (1.1).

E. Extracavity Noise: Shot Noise and Supercontinuum Generation

Typically, individual comb teeth are measured by heterodyning them against a cw laser. Shot noise from the limited power in an individual comb tooth will result in white phase noise of $S_{\varphi n}^{\text{shot noise}}=(\eta/2)N_n$, where η is the detection efficiency, and N_n is the number of photons associated with the nth mode. For a typical detected power of 2 nJ per comb tooth, $S_{\varphi n}^{\text{shot noise}}\sim10^{-10}\,\text{rad}^2/\text{Hz}$, yielding a signal-to-noise ratio (SNR) of 45 dB in a 300 kHz bandwidth and a frequency noise contribution of $S_{\nu n}^{\text{shot noise}}=10^{-10}f^2\,\text{Hz}^2/\text{Hz}$. However, the power per tooth clearly varies strongly with wavelength [see Fig. 7(b) for an example of our supercontinuum spectrum], and therefore so will the shot-noise floor. Moreover, this represents a lower limit to the phase-noise floor, which will likely be limited in practice by the noise generated during the supercontinuum formation, discussed below.

It has been well established in Ti:sapphire frequency combs that there is significant excess amplitude and phase noise generated during supercontinuum broadening in the microstructure fiber, due to the presence of both

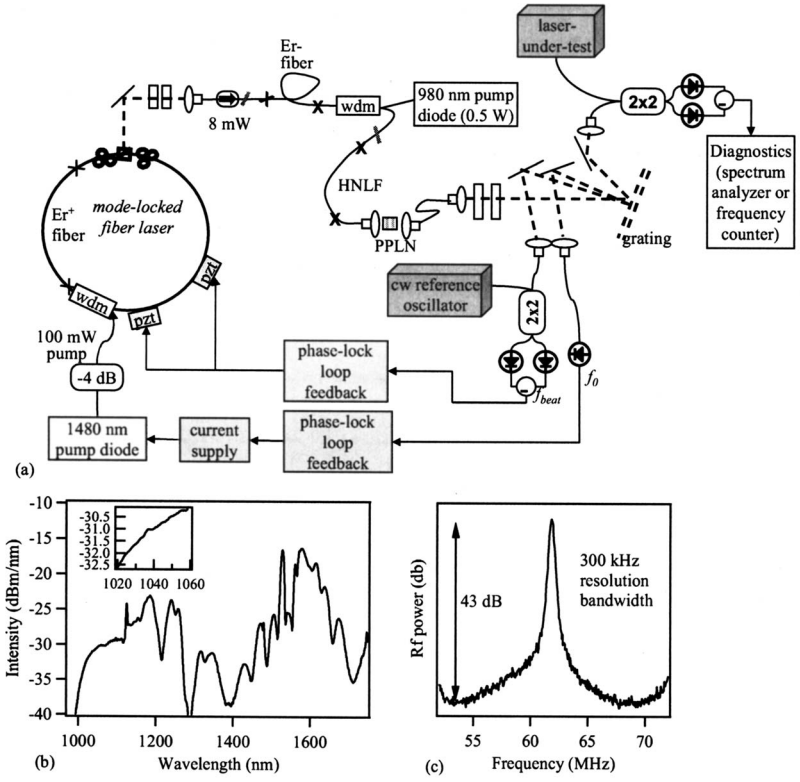

Fig. 7. (a) Schematic of a low-noise fiber-laser frequency comb system. The comb is phase-locked to a cw reference oscillator and used to measure the frequency of a laser under test. For the optical heterodyne measurements, balanced detection is used to enhance the SNR. The laser design uses an air gap as shown in Ref. [12] but all-fiber designs are possible as well. (b) Supercontinuum after periodically poled lithium niobate. Note the enhanced signal at 1037 nm, which is the doubled light from 2074 nm. The enhanced signal at 1126 nm is from a fiber Bragg grating incorporated into the HNLF (Ref. [60]). (c) The unlocked f_0 beat signal from heterodyning the fundamental and doubled 2074 nm light, which has a 43 dB SNR in 300 kHz resolution bandwidth. The uptake on the edges of the beat is a result of the repetition rate beat and another f_0 beat. (There are two such beats in every $f_r=50$ MHz increment.)

low-frequency technical amplitude noise and broadband input shot noise [39–42]. Qualitatively, the same excess noise will be expected for the supercontinuum generation in the highly nonlinear fiber used in fiber frequency combs. Indeed, the basic explanation of the noise generation in microstructure fibers was based on earlier work in noise exploring continuum formation at 1550 nm [57,58]. There are several differences between the fiber comb system and the Ti:sapphire comb system. First, the low-pass filter response of the mode-locked fiber laser can significantly modify the amplitude noise caused by fluctuations in the pump amplitude. This technical amplitude noise may be further modified by the effective frequency response of the subsequent amplifier. Second, in the case of supercontinuum broadening for Ti:sapphire systems, the source of the broadband noise was the input shot noise, whereas here the source of the broadband noise is ASE from the amplifier and the laser gain media. Although there has been no quantitative work to date, qualitatively this ASE will lead to excess phase and amplitude noise on the supercontinuum generated in the HNLF. To the extent the dominant amplitude noise seed is the "flat" ASE from the amplifier and cavity, the resulting phase noise will also be flat, i.e., independent of Fourier frequency f. Under this assumption, the supercontinuum-related noise and shot noise have the same behavior and can be summed

$$S_{\nu n}^{\text{shot noise}}(f) + S_{\nu n}^{\text{supercontinuum}}(f) = Af^2 \quad [\text{Hz}^2/\text{Hz}]. \tag{1.14}$$

The white phase noise floor does not contribute to the linewidth [see Eq. (1.16)], although a raised noise floor will limit the SNR (as illustrated in Fig. 4), which can cause difficulties when "counting" a heterodyne beat or for phase locking the comb since sufficient SNR is needed for the electronic feedback. In Fig. 5, A varies from 10^{-9} to 10^{-10} for SNRs in a 300 kHz bandwidth ranging from 35 to 45 dB.

5. DETAILED COMB CONFIGURATION AND EXPERIMENTAL RESULTS

A detailed schematic of our present comb is given in Fig. 7(a) and follows the general discussion of Section 2. The comb, discussed in some detail in Refs. [11,12,14], is based on a highly stretched-pulse fiber ring laser pumped by 110 mW of light at 1480 nm and produces ~8 mW of output power with f_r of 50 MHz in chirped, ~80 nm wide pulses. No particular special effort was made to reduce the intracavity loss or effective noise figure of the gain medium that might help reduce the ASE-induced quantum limited noise. The effect of pump noise is reduced by operating the pump diode at its maximum rated operating power and then attenuated to the appropriate level [11,12]. The laser rests on a temperature-controlled baseplate and is placed within an enclosure to minimize environmentally induced noise. In addition, the amplifier and HNLF are in a temperature-controlled box to avoid slow changes in fiber birefringence that otherwise must be compensated for by occasionally adjusting the polarization controllers (not shown) before and after the Er amplifier.

The laser pulses are amplified in 50 cm of Er-doped fiber, which is backward-pumped at 980 nm. [A 980 nm pump was chosen to avoid spectrally clipping the amplified pulse from the pump wavelength division multiplexer (WDM).] The amplifier length was chosen by observing the green fluorescence from the Er fiber with an incident laser pulse train and cutting back to the point at which the green fluorescence began to diminish assuming that the gain also began to diminish at that point. The length of the standard single-mode fiber (SMF-28) before (50 cm) and after (40 cm) the Er fiber was selected by minimizing the amplified output pulse duration. The amplified pulse is injected into a 23 cm long piece of UV-treated HNLF [59,60], which generates the supercontinuum [see Fig. 7(b)]. This is followed by a short piece of SMF-28 fiber that provides phase compensation between the 1 and 2 μm ends of the supercontinuum, as required for collinear detection of f_0 [2,46]. The supercontinuum is coupled out of the fiber through a piece of periodically poled lithium niobate to double the 2074 nm light to 1037 nm, and coupled back into single-mode (at 1 μm) optical fiber. The beat between this "doubled" 1037 nm light and the fundamental supercontinuum light at 1037 nm provides f_0 [see Fig. 7(c)].

Depending on the amplifier settings, laser settings, and polarization controller settings, the observed SNR on the f_0 beat signal can vary substantially and reaches the requisite levels to achieve a reasonable phase lock (e.g., 30 dB in 300 kHz bandwidth) only over a fairly narrow range of these operating conditions. Furthermore this SNR must be achieved simultaneously for both the f_0 beat signal and the heterodyne beat signals between the comb and the optical reference as well as any optical source to be measured. These various beat signals are not necessarily optimum under the same conditions and two different approaches have been taken to achieving good SNR simultaneously on all the beat signals. First, the laser output can be split into two branches with two distinct amplifiers and HNLF sections; the output of one branch is used to generate an f_0 beat signal, while the other branch is optimized for the desired spectrum [4]. This two-branch approach is quite robust but comes at the cost of a second amplifier and additional differential phase noise between the two branches. A second approach, followed here, is to use tailored HNLF fiber with UV-induced Bragg gratings to enhance the supercontinuum generation at the desired wavelengths by ~10 dB [60,61]. This second approach comes at the cost of the technical challenge of making the specialty fiber and some loss in measurement flexibility since the specialty fiber will be tailored to specific wavelengths.

In the past, we have used fiber-optic WDMs to split the light for detection; here, however we use a combination of free-space dichroics and gratings to allow for the greatest flexibility in wavelength selection and to minimize out-of-loop path lengths and their associated phase noise. The beat signal between the optical reference and the comb tooth at ν_{nref} is generated by coupling the desired wavelength of comb light selected from the grating back into

single-mode fiber and mixing with the cw reference laser light in a fused fiber coupler. Balanced detection is employed to improve the SNR by increasing the signal power and suppressing any amplitude noise. Figure 8 shows an example of measured frequency noise PSDs for the f_0, and for the comb modes at 1535 and 1126 nm. Also plotted is the fitted frequency noise PSD using Eq. (1.1) from Section 3.

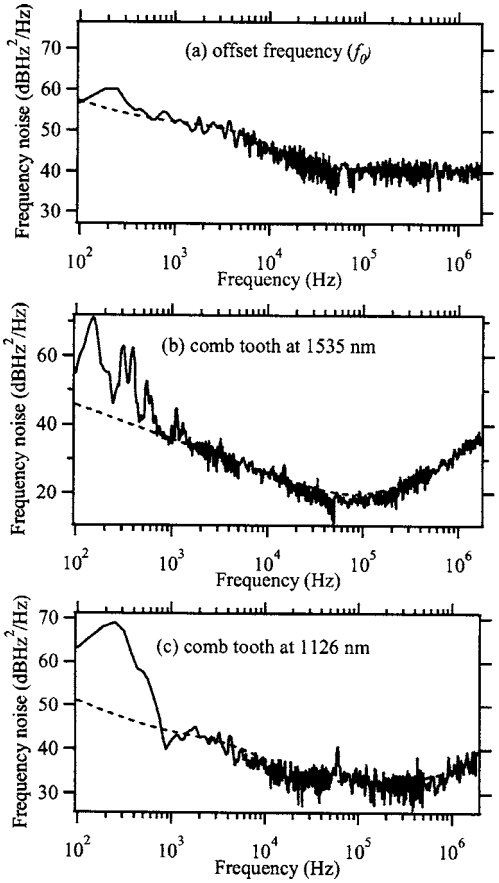

Fig. 8. Free-running frequency noise PSD for the comb mode at (a) f_0 (near 112 MHz), (b) 1535 nm, and (c) 1126 nm as measured by beating the comb against a narrow linewidth cw laser. The solid curve is the measured data and the dashed curve is the fitted data using the model in Section 3 (solid black curve in Fig. 5). The deviations in (b) in the middle frequencies are a result of the complex vibrational spectrum that we have not attempted to model.

To stabilize the comb, we apply feedback to the cavity length and the pump power. A reasonable cavity feedback bandwidth for stabilization of the comb tooth at ν_{nref} is achieved by use of a low-bandwidth (first resonance at 5 kHz), high-dynamic-range fiber stretcher in conjunction with a high-bandwidth (first resonance at 40 kHz), lower-dynamic-range fiber stretcher. The feedback bandwidth for stabilizing the offset frequency through the pump power modulation can be limited by the rolloff in the response of the mode-locked laser to pump power changes at ~5–10 kHz. However, since this response follows a simple low-pass filter, phase-lead compensation can extend the bandwidth to ~80 kHz, and even higher bandwidths should be possible with faster electronics [11,12].

The unlocked and in-loop locked frequency noise PSD for f_0 are compared in Ref. [12], and the unlocked and in-loop locked frequency noise PSD for ν_{nref} are compared in Fig. 9. As discussed in Ref. [14], the integrated phase noise is 1 and 0.35 rad for f_0 and ν_{nref}, respectively, out to 0.5 MHz, with a projected integrated phase noise of 1.3 and 0.5 rad out to the Nyquist frequency of 25 MHz. These tight phase locks also result in a low, counterlimited error on the counted in-loop frequency noise, shown in Fig. 10. The corresponding 10 s stability from these tight locks is below $(0.15\ \text{mHz})/(200\ \text{THz}) = 0.76 \times 10^{-18}$. At these levels, the stability of any measurement will be limited by out-of-loop fiber or air paths necessary to connect the comb light with the laser under test.

6. RESIDUAL NOISE ON A PHASE-LOCKED SYSTEM

We are interested in answering the question: if we measure the in-loop phase-locked frequency noise PSD at f_0

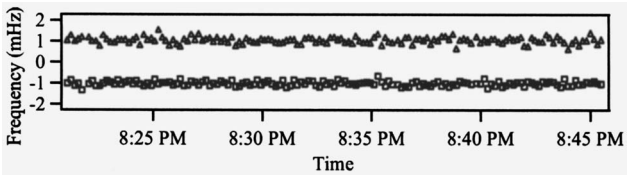

Fig. 10. Counted optical beat signal, shifted to −1 mHz (solid curve) and the counted offset frequency beat signal, shifted to +1 mHz, (dashed curve) for a 10 s gate time. The 150 μHz standard deviation in the counts is due to the frequency counter.

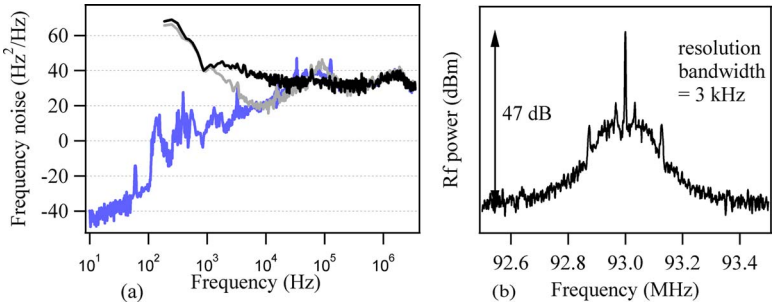

Fig. 9. (Color online) Frequency noise PSD for the comb tooth at 1126 nm for an unlocked comb (solid black curve), a comb with just the offset frequency locked (solid gray curve), and after locking the comb tooth at 1126 nm to the cw laser (solid blue curve). The effect of locking only the offset frequency is the removal of the pump-induced noise, which otherwise dominates for Fourier frequencies from 1 to 10 kHz. The locked and unlocked noise PSD cross at an effective feedback bandwidth of 25 kHz. (b) An example in-loop, phase-locked heterodyne beat signal between the comb tooth near 1126 nm and the laser at 1126 nm for a resolution bandwidth of 3 kHz, corresponding to the blue frequency noise PSD in part (a). The central spike is a coherent peak with an instrument-limited linewidth (below 0.1 Hz).

and ν_{nref}, what can we say about the frequency noise PSD at other frequencies across the comb? First, measurement of the noise on f_0 and ν_{nref}, tells us very little about the *extracavity* noise contributions at other frequencies. The white phase noise floor from shot noise or supercontinuum noise is expected to vary significantly across the comb, and indeed this is observed in the noise floors in Ref. [14]. In addition, extracavity noise from different path lengths for f_0, ν_{nref}, and other ν_n can easily be present, depending on the experimental configuration.

However, measurements of the in-loop frequency noise of f_0 and ν_{nref} do tell us about the *intracavity* noise contributions at other comb modes, ν_n. In terms of the two phase-locked frequencies, f_0 and ν_{nref}, the comb frequencies are $\nu_n = r\nu_{nref} + (1-r)f_0$, where $r \equiv n/n_{ref}$. Therefore, the residual frequency noise PSD at the comb tooth ν_n and Fourier frequency f is $S_{\nu n}(f) = r^2 S_{\nu nref}(f) + (1-r)^2 S_0(f) + 2\chi_n(f) r(1-r)\sqrt{S_{\nu nref}(f) S_0(f)}$, where $-1 < \chi_n(f) < 1$ is the normalized cross-correlation coefficient between the noise on the offset frequency $S_0(f)$ and the noise on the phase-locked comb tooth at $\nu_{nref} S_{\nu nref}(f)$. The first two terms can be written in exactly the form of Eq. (1.2); in other words, they describe noise that increases quadratically from fixed points at 0 THz and ν_{nref}. The cross correlation expresses the fact that the true fixed points may differ. In Ref. [14], ν_{nref} corresponded to 1550 nm, which is very near the fixed point for both quantum noise and pump noise, while the locked $f_0 \sim 100$ MHz was "near" the true fixed point of ~ 1 THz for length fluctuations (at least relative to optical frequencies). Therefore $|\chi| \sim 0$. This fact, in conjunction with the low value of $S_0(f)$, resulted in good agreement when only the first term $S_{\nu n}(f) = r^2 S_{\nu nref}(f)$ was retained. Specifically, if $S_0(f) \ll 4\chi^2 S_{\nu n}(f)$, the cross-correlation term can be safely ignored.

However, in general, in order to calculate the noise on a given tooth $S_{\nu n}(f)$, one needs to know, or at least limit, the values of the cross-correlation coefficient $\chi_n(f)$. For example, if the comb is locked to light at 1126 nm (as in Fig. 9), the lock point is far from any fixed point associated with specific noise terms. Therefore we expect correlations between the residual noise on the offset frequency and optical lock. Indeed Fig. 9 shows the measured frequency noise PSD on the comb at 1126 both with and without the offset frequency phase locked.

Based on the simple parabolic form of the intracavity noise [see Eq. (1.2)], we can make the following general statement regarding $\chi_n(f)$. If the fixed points for the potential noise terms contributing to the residual noise, fall at frequencies within the range of f_0 and ν_{nref} (as is the case for locking the comb to the 1126 nm laser light), then the cross correlation will always be less than zero, $\chi < 0$, and it is a reasonable upper limit to calculate the residual phase noise on the intervening comb teeth using $\chi = 0$. Conversely, if the fixed points for the noise terms fall outside of the range of f_0 and ν_{nref}, then $\chi > 0$. Finally, as stated above, if the fixed points for the noise fall on the two lock points, f_0 and ν_{nref}, as was approximately the case in Ref. [14] then $\chi = 0$.

7. CONCLUSION

In this paper, we have described the design and underlying physics behind a low-noise fiber frequency comb. The comb described here operates with a noise well below that of the quantum limit imposed by the intracavity ASE. For example, from the values in Table 1 and Eq. (1.16), the quantum-limited linewidth is ~ 5 kHz at 1126 nm, whereas the phase-locked linewidth is instrument limited to below 0.1 Hz.

We have based our discussion on our current low-noise, 50 MHz, Er-fiber-laser-based frequency comb. However, most of the values in Table 1 should apply equally well to other Er-fiber-laser-based systems, in particular the fixed points and the frequency dependence should be similar. The magnitude of the noise (the third column in Table 1) will, of course, scale with the external noise source [see Eqs. (1.5), (1.7), (1.9), (1.11), and (1.13)]. Qualitatively, the overall discussion should apply equally well to Yb-based fiber-laser frequency combs. Finally, it is interesting to consider the scaling with repetition frequency (ignoring any thermal effects that may crop up at higher pumping powers.) A useful metric is the comb frequency noise at some specific optical frequency. By Eq. (1.2), we would expect the intracavity noise to scale with the magnitude of the fractional frequency noise on the repetition frequency, $S_r^X(f)$. Assuming a constant pulse energy, for all the intracavity noise sources this fractional noise increases with f_r either linearly or quadratically, which yields a gradual decline in the comb performance as the repetition rate is increased. However, there are many other good reasons to push toward higher repetition frequencies, and such a linear increase in noise power could easily be compensated for by more careful design of a low-noise oscillator.

It is interesting to review why such low-noise fiber-laser frequency comb is possible at all. There are at least three major contributing factors. First, the passive mode-locking mechanism in the laser uses the rapid Kerr nonlinearity in the optical fiber and is extremely effective in locking the relative phases of all participating laser modes despite any perturbations, as indicated by the ability to generate transform-limited 100 fs pulses after correcting for any steady chirp on the output pulse. Therefore, despite the large number of participating laser modes, any noise on the laser cavity perturbs only the modes spacing or offset frequency but not the individual modes separately. Second, unlike a cw fiber laser, a mode-locked fiber laser will not suffer from relaxation oscillations. Instead, the system is overdamped giving a low-pass filter response to pump-power changes [8,9,62] that greatly reduces pump-induced noise at high Fourier frequencies, although the quantum-limited noise does remain. The final critical factor has been the development of specialty fiber with a nonlinearity sufficiently high to allow for continuum generation with low excess phase noise [13,43,60].

The basic prescription for a low-noise frequency comb is fairly clear; it involves reducing the effect of the various noise terms and achieving as high a feedback bandwidth as possible for both the pump-power feedback through faster electronics [12] and the cavity length, possibly by including an electro-optic phase modulator [49]. The most important noise terms are environmental noise at low frequencies, pump noise at intermediate frequencies, quantum- or ASE-driven noise at higher frequencies, and ultimately shot noise and supercontinuum noise at even

higher frequencies. The environmental noise can be reduced by good isolation as with any laser. The pump noise can be reduced by using a low-noise pump, for example, a set of distributed feedback lasers, and by operating the laser with a strong damping, which is expected to increase with higher circulating pulse energies. Stronger damping translates to a lower rolloff frequency $f_{3\,\mathrm{dB}}$ and therefore less sensitivity to pump fluctuations. (For the highest suppression of residual pump-induced noise through feedback, one would like a high feedback bandwidth, which would naively require a high $f_{3\,\mathrm{dB}}$. This contradictory requirement is satisfied by phase-lead compensation that can increase the feedback bandwidth well beyond $f_{3\,\mathrm{dB}}$ [11,12].) The quantum noise is reduced by reducing the cavity loss and increasing the circulating pump power. Finally, it is likely that the supercontinuum noise could be reduced by even higher peak-power pulses or higher nonlinearity fiber, but more work is needed in this area. With future improvements in the laser design, there is no reason that the fiber-laser frequency comb cannot exhibit even lower residual phase noise with an ultimate limit probably set by the supercontinuum noise.

APPENDIX A: NOISE POWER SPECTRAL DENSITY AND LINEWIDTH

The electric field of the comb can be written in terms of a carrier frequency, ν_c, and envelope, $A(t)$, as $E(t) = A(t)\exp(i2\pi\nu_c t)$. For the comb at discrete frequencies ν_n,

$$E(t) = \sum \tilde{A}_n e^{i(2\pi\nu_n + \varphi_n)}, \tag{A1}$$

where the spectrum is given by the frequency-shifted Fourier transform of the envelope function, $\tilde{A}(\nu_n - \nu_c) \equiv \tilde{A}_n \exp(i\varphi_n)$. In the absence of noise, Eq. (A1) describes a sum of perfect cw oscillators. The presence of noise is included by assuming there are slow variations in the envelope function (and carrier frequency) so that the comb structure is maintained but the amplitude, A_n, and phase, φ_n, of each oscillator varies on the "slow" time scale, T [8]. We will ignore the amplitude noise hereafter. The instantaneous frequency of the oscillator is $\nu_n(T) = \nu_n + (2\pi)^{-1}\mathrm{d}\varphi_n(T)/\mathrm{d}T$. As with rf oscillators [50], rather than characterize the noise in the phase, $\varphi_n(T)$, or frequency, $\nu_n(T)$, in time, T, we Fourier transform the noise and square it to arrive at a single-sided PSD for either the phase fluctuations, $S_{\varphi n}(f) = \langle \tilde{\varphi}_n^2 \rangle$ in $\mathrm{rad}^2/\mathrm{Hz}$ or frequency fluctuations, $S_{\nu n}(f) = \langle \tilde{\nu}_n^2 \rangle = f^2 S_{\varphi n}(f)$ in $\mathrm{Hz}^2/\mathrm{Hz}$ as a function of the Fourier frequencies, f for the nth oscillator, where the tilde represents Fourier transform with respect to T and angle brackets indicate a statistical average.

The comb mode FWHM linewidth can be measured by heterodyning the comb with a narrow cw laser and measuring the FWHM of the rf heterodyne beat signal. The linewidth of the comb mode, which is a single number, provides nowhere near as complete a description as the frequency or phase noise PSD, but it is often more experimentally accessible. The linewidth can be derived directly from the phase or frequency PSD, either numerically by integration of the appropriate expression or through standard Monte Carlo techniques (which can be useful in the case that the PSD diverges steeply at zero Fourier frequency). Analytical expressions for simple PSD shapes have also been derived previously and are summarized below [12,50,63–65]:

$$\Delta\nu_n = \pi S_{\nu n}(0)$$
$$\text{for } S_{\nu n}(f) = \text{constant (white frequency noise)},$$

$$\Delta\nu_n = \pi\sqrt{S_{\nu n}(0) f_{3\,\mathrm{dB}}}$$
$$\text{for } S_{\nu n}(f) = \frac{S_{\nu n}(0)}{1 + (f/f_{3\,\mathrm{dB}})^2}, \quad \Delta\nu_n \gg f_{3\,\mathrm{dB}},$$

$$\Delta\nu_n = f_{inst}$$
$$\text{for } S_{\varphi n}(f) = \text{constant} < \ln(2)/f_{Nyq},$$

$$\Delta\nu_n = f_{inst}$$
$$\text{for } \sigma_{\varphi n}^2(f_{inst}/2, f_{Nyq}) < \ln(2),$$
$$f_{inst} = \text{instrument-limited bandwidth},$$

$$\Delta\nu_n = \sqrt{4\ln(2)K[4.3 + \ln(4.3 \times 4\pi^2 K \tau_c^{2.1})]}$$
$$\text{for } S_{\nu n}(f) = K/f, \quad \text{if } (2\pi)^2 K \tau_c \gg 1, \tag{1.16}$$

where $f_{Nyq} = f_r/2$ is the Nyquist frequency and in the last expression τ_c is the observation time. The first expression will be useful for the intracavity ASE-induced noise, the second for the intracavity pump-induced noise, the third for a phase-locked system with white phase noise, the fourth expression is a generalization of the third [63], and the final expression for $1/f$ environmental noise. For our conditions and a cutoff time of 1 ms, the last expression reduces to $\Delta\nu = 5.5[S_{\nu n}(1)]^{1/2}$, used in generating the linewidths for Fig. 6.

ACKNOWLEDGMENTS

We thank Luca Lorini and Jim Bergquist for providing the narrow 1126 nm light used in measuring the unlocked frequency noise on the comb, and John McFerran for assistance in developing the comb. We acknowledge helpful discussions with Ian Coddington, Ingmar Hartl, Ronald Holzwarth, John McFerran, and Qudsia Quraishi. Finally, we benefited greatly from the expertise shared by Scott Diddams, Leo Hollberg and others in their group with regard to low-frequency Ti:sapphire frequency combs.

REFERENCES

1. B. R. Washburn, S. A. Diddams, N. R. Newbury, J. W. Nicholson, M. F. Yan, and C. G. Jørgensen, "Phase-locked erbium-fiber-laser-based frequency comb in the near infrared," Opt. Lett. **29**, 250–252 (2004).
2. T. R. Schibli, K. Minoshima, F.-L. Hong, H. Inaba, A. Onae, H. Matsumoto, I. Hartl, and M. E. Fermann, "Frequency

metrology with a turnkey all-fiber system," Opt. Lett. **29**, 2467–2469 (2004).
3. H. Hundertmark, D. Wandt, N. Haverkamp, and H. R. Telle, "Phase-locked carrier-envelope-offset frequency at 1560 nm," Opt. Express **12**, 770–775 (2004).
4. F. Adler, K. Moutzouris, A. Leitenstorfer, H. Schnatz, B. Lipphardt, G. Grosche, and F. Tauser, "Phase-locked two-branch erbium-doped fiber laser system for long-term precision measurements of optical frequencies," Opt. Express **12**, 5872–5880 (2004).
5. B. R. Washburn, R. Fox, N. R. Newbury, J. W. Nicholson, K. Feder, P. S. Westbrook, and C. G. Jørgensen, "Fiber-laser-based frequency comb with a tunable repetition rate," Opt. Express **12**, 4999–5004 (2004).
6. P. Kubina, P. Adel, F. Adler, G. Grosche, T. W. Hänsch, R. Holzwarth, A. Leitenstorfer, B. Lipphardt, and H. Schnatz, "Long-term comparison of two fiber based frequency comb systems," Opt. Express **13**, 904–909 (2005).
7. I. Hartl, G. Imshev, M. E. Fermann, C. Langrock, and M. M. Fejer, "Integrated self-referenced frequency-comb laser based on a combination of fiber and waveguide technology," Opt. Express **13**, 6490–6496 (2005).
8. N. R. Newbury and B. R. Washburn, "Theory of the frequency comb output from a femtosecond fiber laser," IEEE J. Quantum Electron. **41**, 1388–1402 (2005).
9. B. R. Washburn, W. C. Swann, and N. R. Newbury, "Response dynamics of the frequency comb output from a femtosecond fiber laser," Opt. Express **13**, 10622–10633 (2005).
10. E. Benkler, H. R. Telle, A. Zach, and F. Tauser, "Circumvention of noise contributions in fiber laser based frequency combs," Opt. Express **13**, 5662–5668 (2005).
11. J. J. McFerran, W. C. Swann, B. R. Washburn, and N. R. Newbury, "Elimination of pump-induced frequency jitter on fiber-laser frequency combs," Opt. Lett. **31**, 1997–1999 (2006).
12. J. J. McFerran, W. C. Swann, B. R. Washburn, and N. R. Newbury, "Suppression of pump-induced frequency noise in fiber-laser frequency combs leading to sub-radian f_{ceo} phase excursion," Appl. Phys. B **86**, 219–227 (2007).
13. H. Inaba, Y. Daimon, F. L. Hong, A. Onae, K. Minoshima, T. R. Schibli, H. Matsumoto, M. Hirano, T. Okuno, M. Onishi, and M. Nakazawa, "Long-term measurement of optical frequencies using a simple, robust and low-noise fiber based frequency comb," Opt. Express **14**, 5223–5231 (2006).
14. W. C. Swann, J. J. McFerran, I. Coddington, N. R. Newbury, I. Hartl, M. E. Fermann, P. S. Westbrook, J. W. Nicholson, K. S. Feder, C. Langrock, and M. M. Fejer, "Fiber-laser frequency combs with sub-hertz relative linewidths," Opt. Lett. **31**, 3046–3048 (2006).
15. H. Schnatz, B. Lipphardt, and G. Grosche, "Frequency metrology using fiber-based fs-frequency combs," in *Conference on Lasers and Electro-Optics/Quantum Electronics and Laser Science Conference (CLEO)* (Optical Society of America, 2006), Paper CTuHl.
16. T. Udem, R. Holzwarth, and T. W. Hänsch, "Optical Frequency Metrology," Nature **416**, 233–237 (2002).
17. D. J. Jones, S. A. Diddams, J. K. Ranka, A. Stentz, R. S. Windeler, J. L. Hall, and S. T. Cundiff, "Carrier-envelope phase control of femtosecond mode-locked lasers and direct optical frequency synthesis," Science **288**, 635–639 (2000).
18. S. A. Diddams, Th. Udem, J. C. Bergquist, E. A. Curtis, R. E. Drullinger, L. Hollberg, W. M. Itano, W. D. Lee, C. W. Oates, K. R. Vogel, and D. J. Wineland, "An optical clock based on a single trapped $^{199}Hg^{+}$ ion," Science **293**, 825–828 (2001).
19. L.-S. Ma, Z. Bi, A. Bartels, L. Robersson, M. Zucco, R. S. Windeler, G. Wilpers, C. Oates, L. Hollberg, and S. A. Diddams, "Optical frequency synthesis and comparison with uncertainty at the 10^{-19} level," Science **303**, 1843–1845 (2004).
20. K. Minoshima and H. Matsumoto, "High-accuracy measurement of 240-m distance in an optical tunnel by use of a compact femtosecond laser," Appl. Opt. **39**, 5512–5517 (2000).
21. R. W. Fox, B. R. Washburn, N. R. Newbury, and L. Hollberg, "Wavelength references for interferometry in air," Appl. Opt. **44**, 7793–7801 (2005).
22. W. C. Swann and N. R. Newbury, "Frequency-resolved coherent lidar using a femtosecond fiber laser," Opt. Lett. **31**, 826–828 (2006).
23. K. W. Holman, D. D. Hudson, J. Ye, and D. J. Jones, "Remote transfer of a high-stability and ultralow-jitter timing signal," Opt. Lett. **30**, 1225–1227 (2005).
24. C. Daussy, O. Lopez, A. Amy-Klein, A. Goncharov, M. Guinet, C. Chardonnet, F. Narbonneau, M. Lours, D. Chambon, S. Bize, A. Clairon, G. Santarelli, M. E. Tobar, and A. N. Luiten, "Long-distance frequency dissemination with a resolution of 10(−17)," Phys. Rev. Lett. **94**, 203904 (2005).
25. J. J. McFerran, E. N. Ivanov, A. Bartels, G. Wilpers, C. W. Oates, S. A. Diddams, and L. Hollberg, "Low-noise synthesis of microwave signals from an optical source," Electron. Lett. **41**, 650–651 (2005).
26. Menlo Systems GmBH, www.menlosystems.com.
27. Toptica photonics, www.toptica.com.
28. L. E. Nelson, D. J. Jones, K. Tamura, H. A. Haus, and E. P. Ippen, "Ultrashort-pulse fiber ring lasers," Appl. Phys. B **65**, 277–294 (1997).
29. K. Tamura, E. P. Ippen, H. A. Haus, and L. E. Nelson, " 77-fs pulse generation from a stretched-pulse mode-locked all-fiber ring laser," Opt. Lett. **18**, 1080–1083 (1993).
30. J. Rauschenberger, T. M. Fortier, D. J. Jones, J. Ye, and S. T. Cundiff, "Control of the frequency comb from a mode-locked erbium-doped fiber laser," Opt. Express **10**, 1404–1410 (2002).
31. F. Tauser, A. Leitenstorfer, and W. Zinth, "Amplified femtosecond pulses from an Er:fiber system: nonlinear pulse shortening and self-referencing detection of the carrier-envelope phase evolution," Opt. Express **11**, 594–600 (2003).
32. F.-L. Hong, K. Minoshima, A. Onae, H. Inaba, H. Takada, A. Hirai, H. Matsumoto, T. Sugiura, and M. Yoshida, "Broad-spectrum frequency comb generation and carrier-envelope offset frequency measurement by second harmonic generation of a mode-locked fiber laser," Opt. Lett. **28**, 1–3 (2003).
33. J. Ye, J. L. Hall, and S. A. Diddams, "Precision phase control of an ultrawide-bandwidth femtosecond laser: a network of ultrastable frequency marks across the visible spectrum," Opt. Lett. **25**, 1675–1677 (2000).
34. S. R. Bramwell, D. M. Kane, and A. I. Ferguson, "Frequency offset locking of a synchronously pumped mode-locked dye laser," Opt. Commun. **56**, 112–116 (1985).
35. A. Bartels, C. W. Oates, L. Hollberg, and S. A. Diddams, "Stabilization of femtosecond laser frequency combs with subhertz residual linewidths," Opt. Lett. **29**, 1081–1083 (2004).
36. H. A. Haus and A. Mecozzi, "Noise of mode-locked lasers," IEEE J. Quantum Electron. **29**, 983–996 (1993).
37. R. Paschotta, "Noise of mode-locked lasers (Part II): timing jitter and other fluctuations," Appl. Phys. B **79**, 163–173 (2004).
38. R. Paschotta, A. Schlatter, S. C. Zeller, H. R. Telle, and U. Keller, "Optical phase noise and carrier-envelope offset noise of mode-locked lasers," Appl. Phys. B **82**, 265–273 (2006).
39. K. L. Corwin, N. R. Newbury, J. M. Dudley, S. Coen, S. A. Diddams, K. Weber, and R. S. Windeler, "Fundamental noise limitations to supercontinuum generation in microstructure fiber," Phys. Rev. Lett. **90**, 113904 (2003).
40. K. L. Corwin, N. R. Newbury, J. M. Dudley, S. Coen, S. A. Diddams, B. R. Washburn, K. Weber, and R. S. Windeler, "Fundamental amplitude noise limitations to

supercontinuum spectra generated in microstructure fiber," Appl. Phys. B **77**, 269–277 (2003).
41. N. R. Newbury, B. R. Washburn, K. L. Corwin, and R. S. Windeler, "Noise amplification during supercontinuum generation in microstructure fiber," Opt. Lett. **28**, 944–946 (2002).
42. B. R. Washburn and N. R. Newbury, "Phase, timing, and amplitude noise on supercontinua generated in microstructure fiber," Opt. Express **12**, 2166–2175 (2004).
43. J. W. Nicholson, M. F. Yan, P. Wisk, J. Fleming, F. DiMarcello, E. Monberg, A. Yablon, C. G. Jørgensen, and T. Veng, "All-fiber, octave-spanning supercontinuum," Opt. Lett. **28**, 643–645 (2003).
44. J. W. Nicholson, P. S. Westbrook, K. S. Feder, and A. D. Yablon, "Supercontinuum generation in UV irradiated fibers," Opt. Lett. **29**, 2363–2365 (2004).
45. H. R. Telle, G. Steinmeyer, A. E. Dunlop, J. Stenger, D. H. Sutter, and U. Keller, "Carrier-envelope offset phase control: a novel concept for absolute optical frequency and ultrashort pulse generation," Appl. Phys. B **69**, 327–332 (1999).
46. I. Hartl, T. R. Schibili, G. Imbeshev, G. C. Cho, M. N. Fermann, K. Minoshima, A. Onae, F.-L. Hong, H. Matsumoto, J. W. Nicholson, and M. F. Yan, "Carrier envelope phase locking of an in-line, low-noise Er fiber system," in *Conference on Lasers and Electro-Optics* (Optical Society of America, 2004), p. 59.
47. N. Haverkamp, H. Hundertmark, C. Fallnich, and H. R. Telle, "Frequency stabilization of mode-locked erbium fiber lasers using pump power control," Appl. Phys. B **78**, 321–324 (2004).
48. H. R. Telle, B. Lipphardt, and J. Stenger, "Kerr-lens, mode-locked lasers as transfer oscillators for optical frequency measurements," Appl. Phys. B **74**, 1–6 (2002).
49. D. D. Hudson, K. W. Holman, R. J. Jones, S. T. Cundiff, J. Ye, and D. J. Jones, "Mode-locked fiber laser frequency-controlled with an intracavity electro-optic modulator," Opt. Lett. **30**, 2948–2950 (2005).
50. D. B. Sullivan, D. W. Allan, D. A. Howe, and F. L. Walls, eds. "Characterization of clocks and oscillators," NIST Technical Note 1337 (NIST, 1990).
51. H. A. Haus and E. P. Ippen, "Group velocity of solitons," Opt. Lett. **26**, 1654–1656 (2001).
52. C. J. McKinstrie, J. Santhanam, and G. P. Agrawal, "Grodon–Haus timing jitter in dispersion-managed systems with lumped amplification: analytical approach," J. Opt. Soc. Am. B **19**, 640–649 (2002).
53. A. Schlatter, B. Rudin, S. C. Zeller, R. Paschotta, G. J. Spuhler, L. Krainer, N. Haverkamp, H. R. Telle, and U. Keller, "Nearly quantum-noise-limited timing jitter from miniature Er:Yb:glass lasers," Opt. Lett. **30**, 1536–1538 (2005).
54. E. Desurvire, *Erbium-Doped Fiber Amplifiers* (Wiley, 1994).
55. H. A. Haus, "Quantum noise in a solitonlike repeater system," J. Opt. Soc. Am. B **8**, 1122–1126 (1991).
56. P. T. Ho, "Phase and amplitude fluctuations in a mode-locked laser," IEEE J. Quantum Electron. **21**, 1806–1813 (1985).
57. M. Nakazawa, K. Tamura, H. Kubota, and E. Yoshida, "Coherence degradation in the process of supercontinuum generation in an optical fiber," Opt. Fiber Technol. **4**, 215–223 (1998).
58. H. Kubota, K. R. Tamura, and M. Nakazawa, "Analyses of coherence-maintained ultrashort optical pulse trains and supercontinuum generation in the presence of soliton-amplified spontaneous-emission interaction," J. Opt. Soc. Am. B **16**, 2223–2232 (1999).
59. P. S. Westbrook, J. W. Nicholson, K. Feder, and A. D. Yablon, "UV processing of highly nonlinear fibers for enhanced supercontinuum generation," in *Optical Fiber Conference* (Optical Society of America, 2004).
60. P. S. Westbrook, J. W. Nicholson, K. S. Feder, Y. Li, and T. Brown, "Supercontinuum generation in a fiber grating," Appl. Phys. Lett. **85**, 4600–4602 (2004).
61. K. Kim, S. A. Diddams, P. S. Westbrook, J. W. Nicholson, and K. S. Feder, "Improved stabilization of a 1.3 μm femtosecond optical frequency comb by use of a spectrally tailored continuum from a nonlinear fiber grating," Opt. Lett. **31**, 277–279 (2006).
62. S. Namiki, E. P. Ippen, H. A. Haus, and K. Tamura, "Relaxation oscillation behavior in polarization additive pulse mode-locked fiber ring lasers," Appl. Phys. Lett. **69**, 3969–3971 (1996).
63. F. L. Walls and A. DeMarchi, "RF spectrum of a signal after frequency multiplication; measurement and comparison with a simple calculation," IEEE Trans. Instrum. Meas. **IM-24**, 210–217 (1975).
64. D. S. Elliott, R. Roy, and S. J. Smith, "Extracavity laser band-shape and bandwidth modification," Phys. Rev. A **26**, 12–18 (1982).
65. L. B. Mercer, "1/f frequency noise effects on self-heterodyne linewidth measurements," J. Lightwave Technol. **9**, 485–493 (1991).